

# **Fuelfinder: Remote Leak Detector for Liquid Hydrocarbons**

## **Final Report**

Contract Number: DTPH56-10-T-000017

Prepared by:

Mark G. Allen, Richard T. Wainner, Mickey B. Frish  
Physical Sciences Inc.  
20 New England Business Center  
Andover, MA 01810-1077

Prepared for:

U.S. Department of Transportation/PHMSA  
120 New Jersey Avenue, SE  
Washington, DC 20590

November 2018

This research was funded in part under the Department of Transportation, Pipeline and Hazardous Materials Safety Administration's Pipeline Safety Research and Development Program. The views and conclusions contained in this document are those of the authors and should not be interpreted as representing the official policies, either expressed or implied, of the Pipeline and Hazardous Materials Safety Administration, or the U.S. Government.

## TABLE OF CONTENTS

<u>Section</u>	<u>Page</u>
1. Impact from Research Results .....	1
2. Gasoline Vapor MWIR Absorption .....	2
3. Simulation of Fuelfinder Response at Target Wavelengths .....	3
4. Experimental Validation of Fuelfinder Response Simulation .....	8
5. ICL Testing .....	12
6. Laboratory Demonstration of Fuelfinder Response.....	13
7. Summary and Suggested Next Steps .....	18

## LIST OF FIGURES

<u>Figure No.</u>	<u>Page</u>
Figure 1. Relative absorption spectra of individual components of gasoline. ....	2
Figure 2. Composite absorption spectra showing gasoline vapor blends, atmospheric interferences, and target wavelength regions of interest. ....	3
Figure 3. Detailed spectral simulation of gasoline vapor and atmospheric methane/water vapor, and target wavelength regions of interest. ....	5
Figure 4. Normalized 2f returned power as a function of modulation depth for spectral region c. ....	6
Figure 5. Detection limit for pure gasoline vapor detection at selected target ranges. ....	7
Figure 6. Detection limits for selected spectral regions when sensor noise include amplitude of 0 - 600,000 ppm-m water vapor uncertainty. ....	8
Figure 7. Comparison of available ICL tuning range (bottom) with absorption spectra of several standard gases. ....	9
Figure 8. Experimental setup for sensor simulation validation. ....	9
Figure 9. Survey absorption spectra of ethylene at various laser heater setpoints compared to HITRAN simulation. ....	10
Figure 10. Example laser scan waveform through the absorption with and with-out ethylene at a total cell pressure of 760 Torr (balance nitrogen). ....	11
Figure 11. Comparison of experimental (solid) and modeled (dashed) dependence of WMS 1f and 2f signals with laser modulation amplitude using the ethylene absorption feature at $2986.8 \text{ cm}^{-1}$ . ....	12
Figure 12. (left) Laser spectral sensitivity to operating temperature and drive current. (right) Laser output power versus operating temperature and drive current. ....	13
Figure 13. Schematic of laboratory prototype Fuelfinder backscatter experiment. ....	13
Figure 14. Recorded traces of the ICL scatter signals with (blue) and without (red) an etalon in the beam path. ....	14
Figure 15. Photo of the laboratory prototype transceiver (cover partially off) with 2 cm optical cell in front of the outgoing beam, and connected to the gasoline vapor delivery system (background). ....	15
Figure 16. (top) Recorded oscilloscope traces (100-sweep (0.1sec) average) for 4 noted conditions. (bottom) Calculated absorbance for the two conditions with gasoline in the path of the laser beam. ....	16
Figure 17. (top) Recorded oscilloscope traces (blue) (100-sweep (0.1 sec) average) and sine fit (red) for 3 different fuel concentrations in the optical cell. (bottom) Residuals from the fits. Note the 2f content. Also evident is the sharp water feature at the wings. ....	17

## LIST OF FIGURES (Continued)

<u>Figure No.</u>		<u>Page</u>
Figure 18.	Lock-in quadrature signals for $2f$ at different gasoline concentrations. The signals are normalized by the simultaneously recorded $1f$ magnitude. Signals at the zero gasoline condition ( $2f / 1f$ “offset”) are indicated and increasing gasoline directs the signal in the direction of the arrows. The green data points are simply the orange data with the offset subtracted. ....	17
Figure 19.	Plot of offset-corrected $2f / 1f$ signals versus calculated gasoline concentration in the optical cell.....	18

# Final Report

Date of Report: *November 11, 2018*

Contract Number: *DTPH56-10-T-000017*

Prepared for: *Department of Transportation*

Project Title: *Fuelfinder: Remote Leak Detector for Liquid Hydrocarbons*

Prepared by: *Physical Sciences Inc.*

Contact Information: *Mark G. Allen ([allen@psicorp.com](mailto:allen@psicorp.com), 978.738.8131)*

## 1. Impact from Research Results

The Fuelfinder program supported R&D efforts to develop a prototype handheld mid-IR stand-off sensor for early detection of hydrocarbon leaks from buried pipelines. The technical basis for the sensor is an extension of PSI's commercial near-IR methane leak detector, RMLD. In the Fuelfinder configuration, the RMLD near-IR laser and detector components are replaced by mid-IR equivalents, including recently available Interband Cascade Laser (ICL) capability. PSI's licensed commercial supplier of the RMLD, Heath Consultants, assisted PSI in defining a manufacturable product configuration that meets the needs of the user community. Kinder-Morgan, one of the largest owners of pipeline distribution systems in the US, assisted PSI in understanding typical leak scenarios and operational constraints.

During the course of the program, PSI completed a detailed spectroscopic study of gasoline vapor, determining the majority constituent components and selected several target spectral regions for the ICL. A complete system simulation tool to predict the Fuelfinder's response for various application scenarios was developed and validated against laboratory testing. After nearly 20 months delay, a commercial supplier for the ICL succeeded in producing a laser that operates at wavelengths within some of our target spectral regions. This laser was used to complete a demonstration of a laboratory prototype Fuelfinder sensor in a stand-off detection configuration. The sensor demonstrated linear response to gasoline vapor concentration and a noise-equivalent detection limit of ~10 ppm-m.

This is the first ever demonstration of a room-temperature diode-laser-based sensor for measurement of gasoline vapor. The laboratory detection limits are consistent with our detailed sensor performance simulations. The program has produced results that support the development of an advanced prototype sensor for use in field studies of the sub-surface transport and above-surface vapor plumes associated with buried pipeline leaks.

## 2. Gasoline Vapor MWIR Absorption

Gasoline is a mixture of many hydrocarbon constituents, each with different vapor pressure and diffusivities. While there is some variability in specific gasoline composition depending on brand, winter/summer mixes, and regular/premium grades, we can generally note that gasoline is approximately 60 -70% alkanes, 25 – 30% aromatics, and 6-9% alkenes. When considering a specific liquid composition mix and associated vapor pressure of each constituent, we find that the predominant vapor phase species in equilibrium (i.e. for an infinite reservoir of chemical stable liquid) are iso-pentane (40-50% vapor phase composition) and n-butane (20 – 25%). These short-chain alkanes have low water solubility<sup>1,2</sup> and are expected to volatilize rapidly, making their way toward the surface through fissures and natural soil porosity.

Using FTIR IR spectral databases for the individual chemical constituents, we can see the rich spectral content of the major species, as shown in Figure 1. Assuming that all of these components are present in their equilibrium composition, we can calculate a total absorption spectrum as shown in Figure 2.

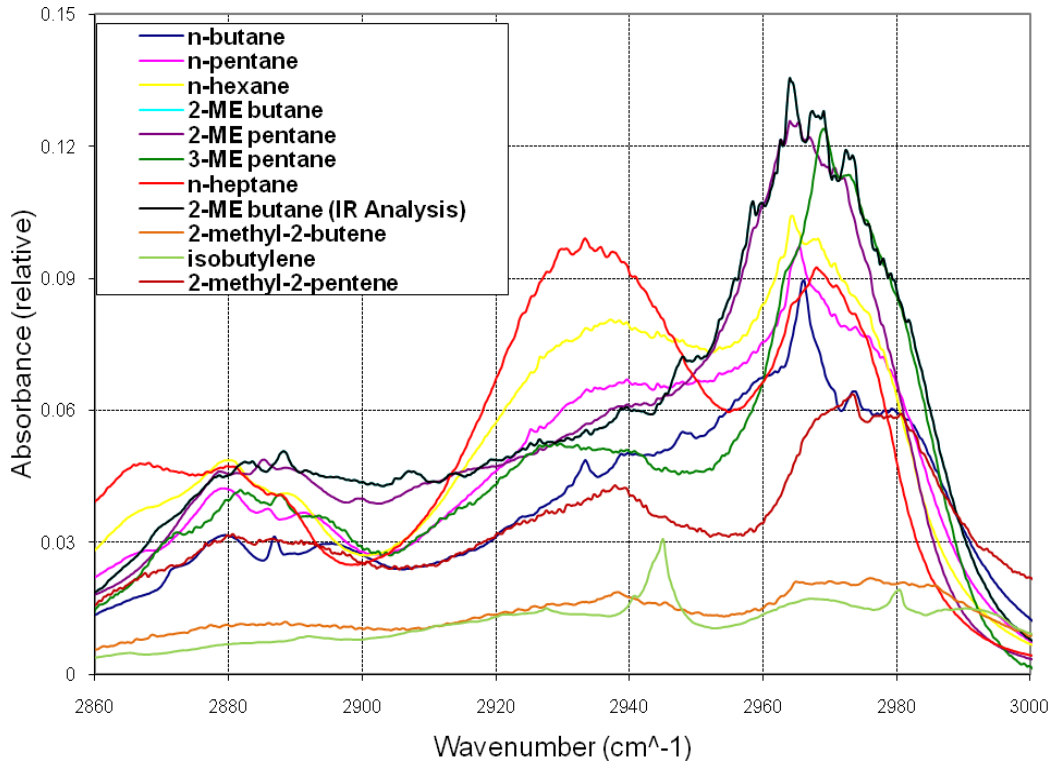


Figure 1. Relative absorption spectra of individual components of gasoline.

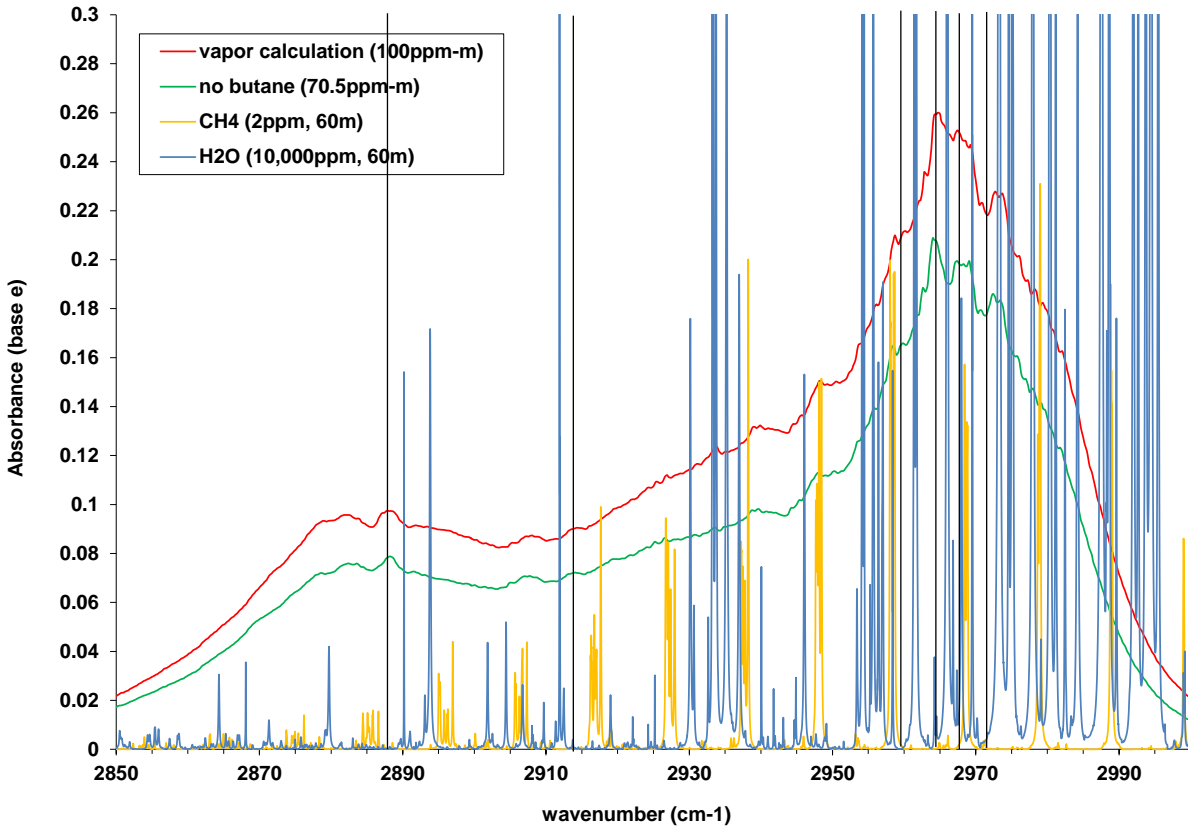


Figure 2. Composite absorption spectra showing gasoline vapor blends, atmospheric interferences, and target wavelength regions of interest.

In Figure 2, the red curve is the composite absorption spectrum for a pathlength-concentration product of 100 ppm-m of equilibrium gasoline vapor. The green curve is a composite with the butane portion (29.5 ppm-m) removed. The orange transitions are the methane transitions in this region for a typical atmosphere and an assumed round-trip pathlength of 60 m. The blue transitions are for 10,000 ppm water vapor over the same pathlength.

### 3. Simulation of Fuelfinder Response at Target Wavelengths

Seven regions of the composite gasoline absorption spectrum were selected by visual inspection for a large 2<sup>nd</sup> derivative component on the gasoline vapor and their relative immunity from absorption interference by atmospheric water vapor. Characteristics of the 7 regions are summarized in Table 1 and 5 of the seven are shown in the simulated absorption spectrum of Figure 3.

Table 1. Summary Candidate Spectral Regions

Region	$\Delta\nu$ (cm <sup>-1</sup> )	2f response (mW / Wdc)		Ratio	Effective $k_{2(\text{fuel})}$
		Fuel	H <sub>2</sub> O		
a	0.41	0.8	-0.8	-1	0.401
b	0.25	1.4	-0.2	-7	0.215
c	1.0	8.0	1.4	6	0.617
d	0.2	0.3	-0.1	-3	0.124
e	0.5	-1.0	0.06	-17	0.171
f	1.1	0.7	0.08	9	0.596
g	1.5	1.9	-0.6	-3	0.377

The entries in Table 1:

- $\Delta\nu$  = amplitude of optimized laser modulation parameter (half-width of spectral window, cm<sup>-1</sup>)
- 2f response = value of the 2<sup>nd</sup> harmonic response (signed to include phase) of the fuel and water vapor contribution
- Ratio = the ratio of the 2f response of fuel to water vapor (a measure of the relative strength of the two signals)
- Effective  $k_{2(\text{fuel})}$  = an effective lineshape function factor indicating the relative strength of the 2f response to that of an analytical calculation for optimal modulation over a Lorentzian lineshape, which has  $k_2=2.2$ .

For Figure 3, the gasoline vapor was assumed to be at a column density of 100 ppm-m, the methane at standard atmospheric concentrations of 2 ppm, water vapor at 10,000 ppm (approximately 25% relative humidity at 30 C), and a 60 m round-trip path.

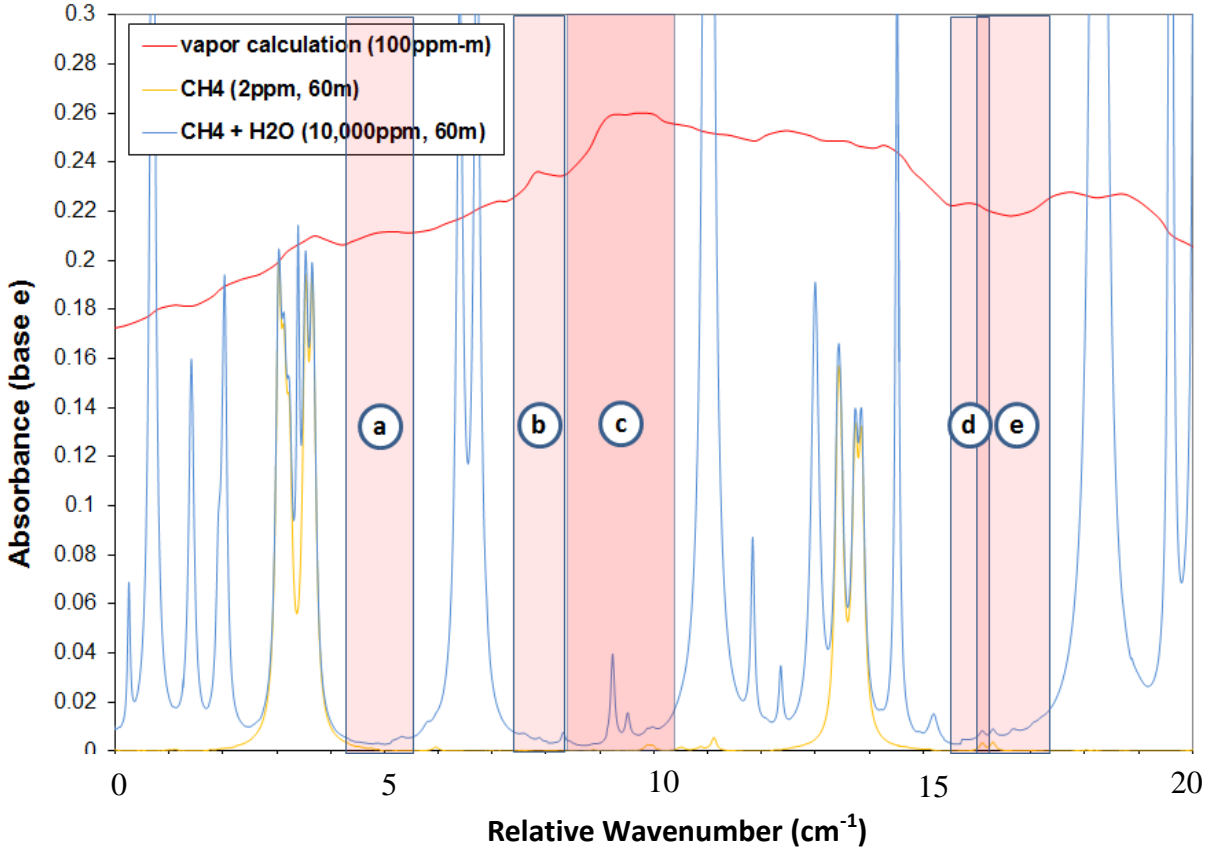


Figure 3. Detailed spectral simulation of gasoline vapor and atmospheric methane/water vapor, and target wavelength regions of interest.

We first investigated the optimum wavelength modulation depth (half-width of spectral windows in Figure 3) to maximize the ratio of the fuel signal to the background interference. Figure 4 shows one example plot of the fuel (100 ppm-m), background (600,000 ppm-m H<sub>2</sub>O), and fuel+background signals as a function of modulation depth for the spectral region c in Figure 3. The fuel signal increases smoothly with modulation depth up to about 1.3 cm<sup>-1</sup>, reflecting the approximate spectral width of the feature. There are two nearby water lines that create spectral interferences: one has a much narrower spectral width, and so its contribution decreases with increasing modulation depth, while the other has a much broader curvature whose contribution will increase with increasing modulation depth but in the negative direction due to its negative curvature.

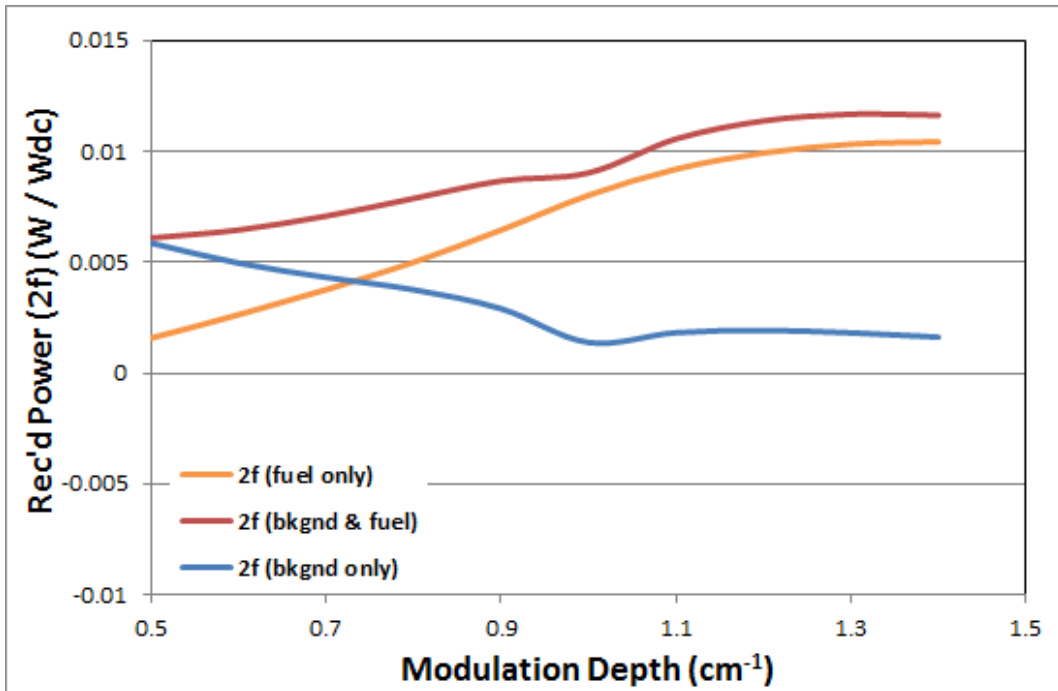


Figure 4. Normalized 2f returned power as a function of modulation depth for spectral region c.

Since the atmospheric background is an uncontrolled interference, we seek a modulation depth where the ratio of the fuel/background is maximized, consistent with a practical constraint on the maximum modulation depth capability of the laser itself. For this target region, that optimum is near a modulation depth of  $1.0 \text{ cm}^{-1}$ . Similar studies were conducted in each spectral region in order to select the modulation depth tabulated in Table 1. Figure 5 is summary plot of the detection limit of a model Fuelfinder unit assuming a 25 mW ICL, an InAs detector cooled to  $-40\text{C}$ , and a typical hand-held collection optic aperture of 4" for each of the spectral windows. For this plot, the signal used is that of gasoline vapor alone, without any water vapor interferences. For this idealized situation, detection limits below 10 ppm-m are possible at target ranges out to 30 m.

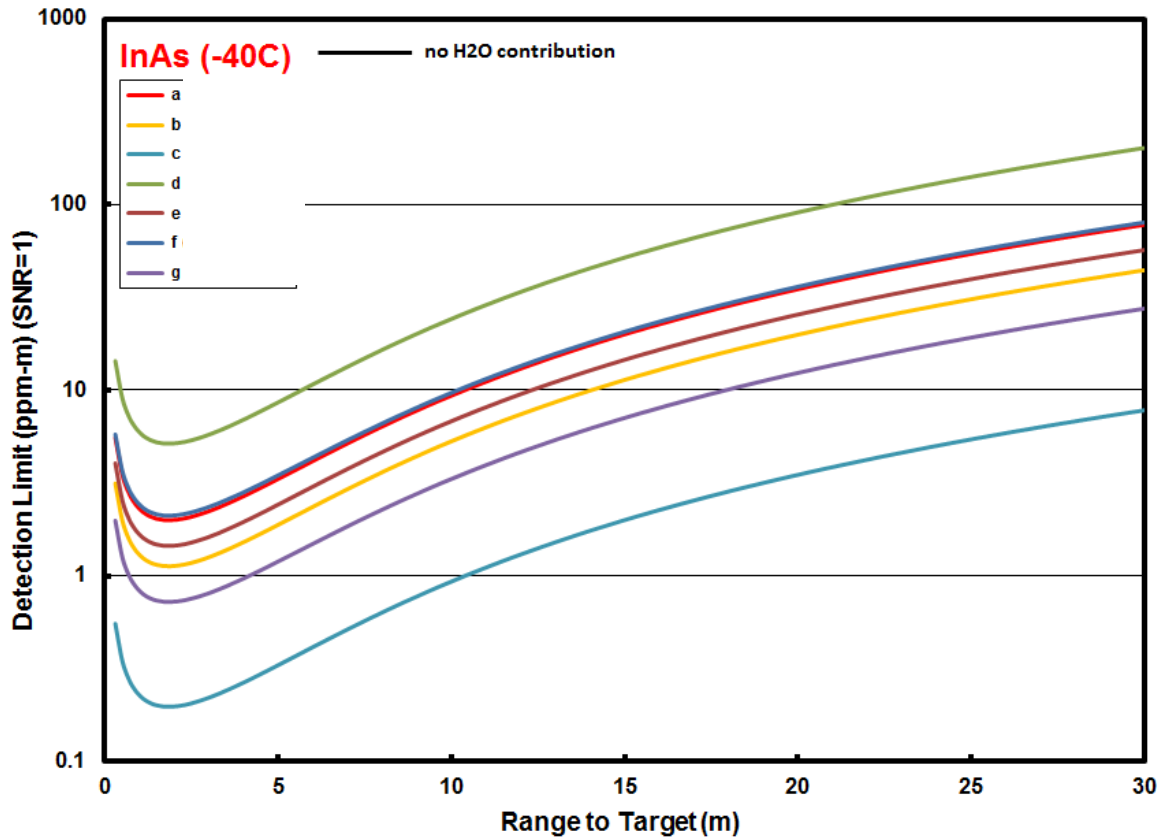


Figure 5. Detection limit for pure gasoline vapor detection at selected target ranges.

We can quantify the effect of the uncontrolled atmospheric background (all due to water vapor in the cases described from here on) by comparing the sensor's response to an atmosphere containing no interference and with interference of 600,000 ppm-m (or 10,000 ppm distributed over a 60 m round-trip path). Figure 6 is a comparison of the idealized pure gasoline vapor detection limit to a condition where the sensor noise includes the amplitude change of the  $2f$  signal associated with a 0 - 600,000 ppm-m change in the water vapor concentration along the line-of-sight.

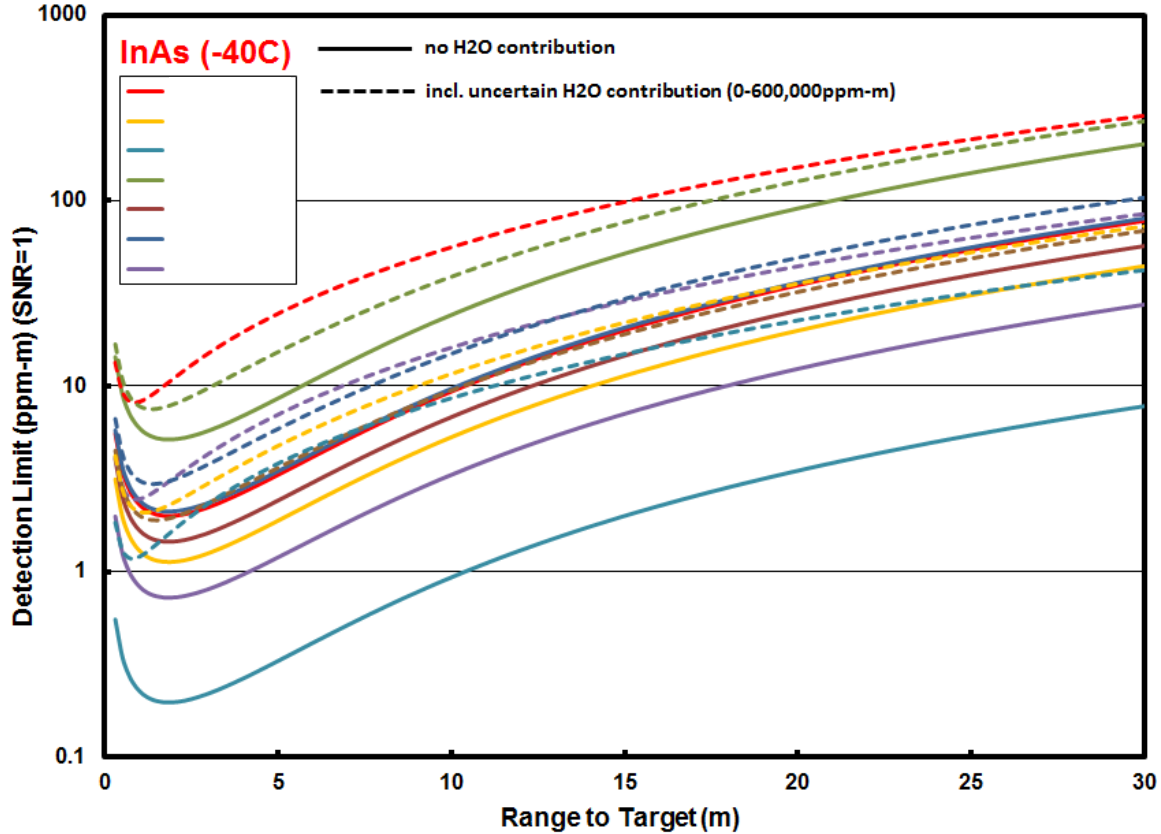


Figure 6. Detection limits for selected spectral regions when sensor noise include amplitude of 0 - 600,000 ppm-m water vapor uncertainty.

From Figure 6, we see that most sensitive spectral region for fuel vapor (f), is also the most sensitive to spurious clutter from uncontrolled changes in ambient humidity, which result in an order of magnitude increase in the detection limit. Spectral region e, in contrast, has the minimum impact on detection limit due to the water vapor clutter, while preserving detection limits 10-ppm for ranges up to 15 m. Based on these considerations, spectral regions e, b, and g, in order of decreasing priority, were selected for the target ICL fabrication or purchase.

#### 4. Experimental Validation of Fuelfinder Response Simulation

Prior to purchasing an ICL suitable for gasoline vapor detection, we validated our design tool against experimental data in controlled laboratory experiments. Toward that end, we assembled a laboratory setup using an available cryogenically-cooled ICL. Figure 7 plots the tuning range of the ICL central frequency as a function of injection current (bottom) along with the absorption spectra of several easily handled laboratory standards. From this analysis, we have selected the ethylene feature near  $2987\text{ cm}^{-1}$  as the test feature against which we validated our sensor simulation tool.

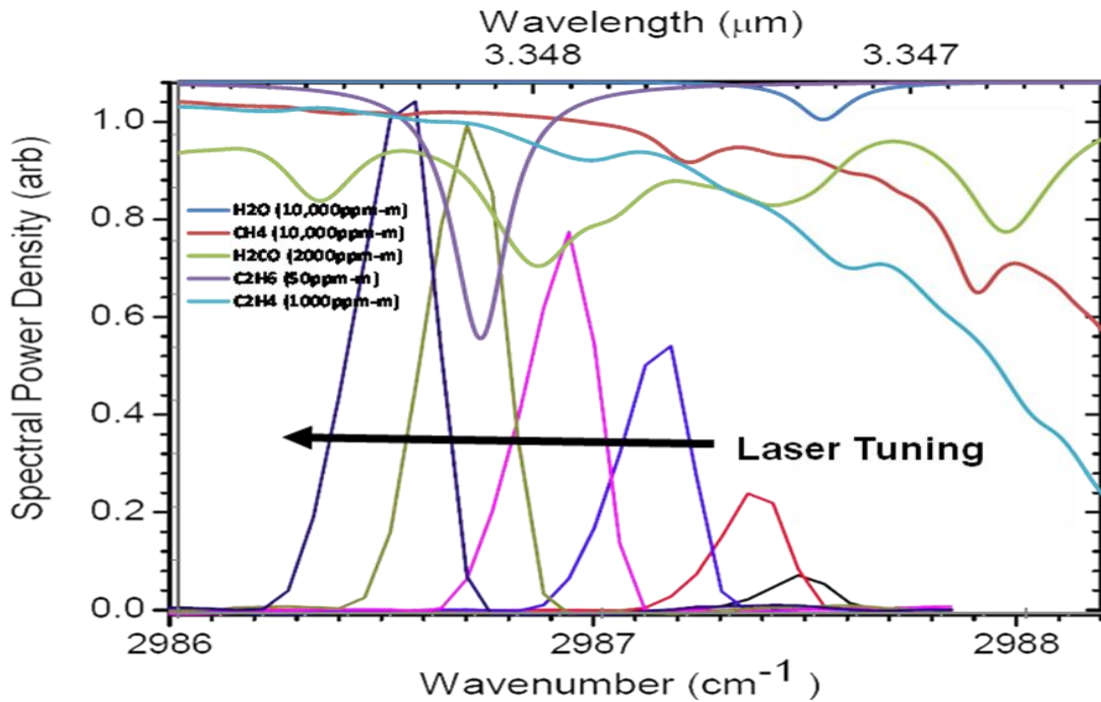


Figure 7. Comparison of available ICL tuning range (bottom) with absorption spectra of several standard gases.

The experimental setup for these validation studies is shown in Figure 8. Controlled mixtures of pure ethylene and nitrogen were introduced into a 50 cm length absorption cell with variable total pressure operation. The ICL output was collimated and directed through the cell. The beam was expanded after the cell to avoid saturation of the InSb detector. The ethylene detection limits as a function of modulation depth were experimentally determined and compared to the sensor simulation results to validate the simulation tool.

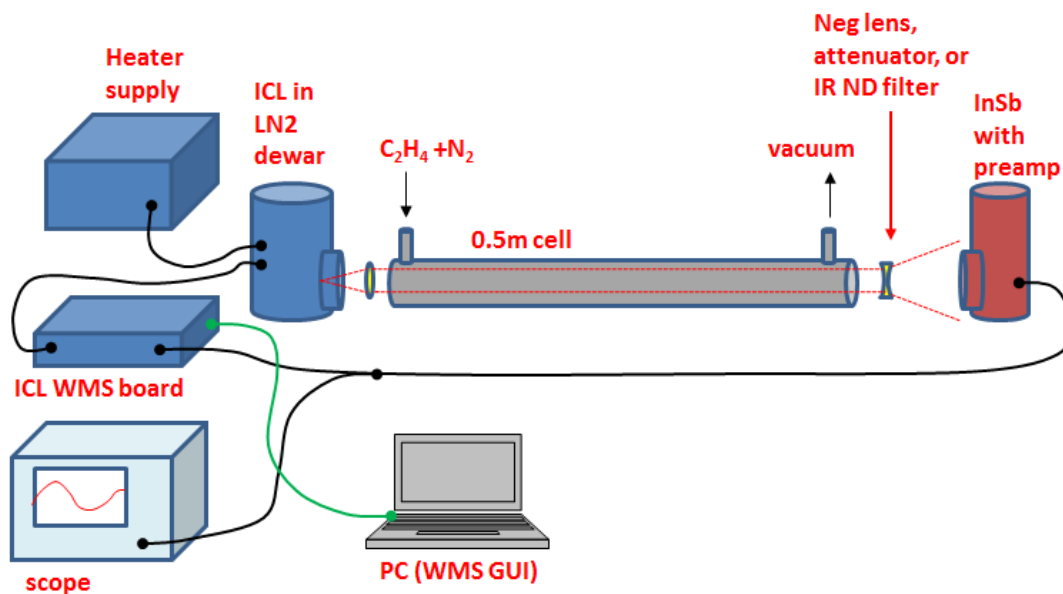


Figure 8. Experimental setup for sensor simulation validation.

In order to calibrate the absolute wavelength of the ICL as a function of injection current and temperature, a survey spectrum of 35 Torr pure ethylene in the cell was conducted and is shown in Figure 9. The dashed red line is the HITRAN simulation of the ethylene spectrum and each solid color curve represents an injection-current ramp of the laser output wavelength at various temperature setpoints (the actual temperature was not measured or regulated in this simple setup, but is proportional to the noted heater control voltage in the plot). The absorption scans as a function of time so recorded are adjusted with scale and bias to overlay the simulation, providing a direct calibration of the laser output wavelength.

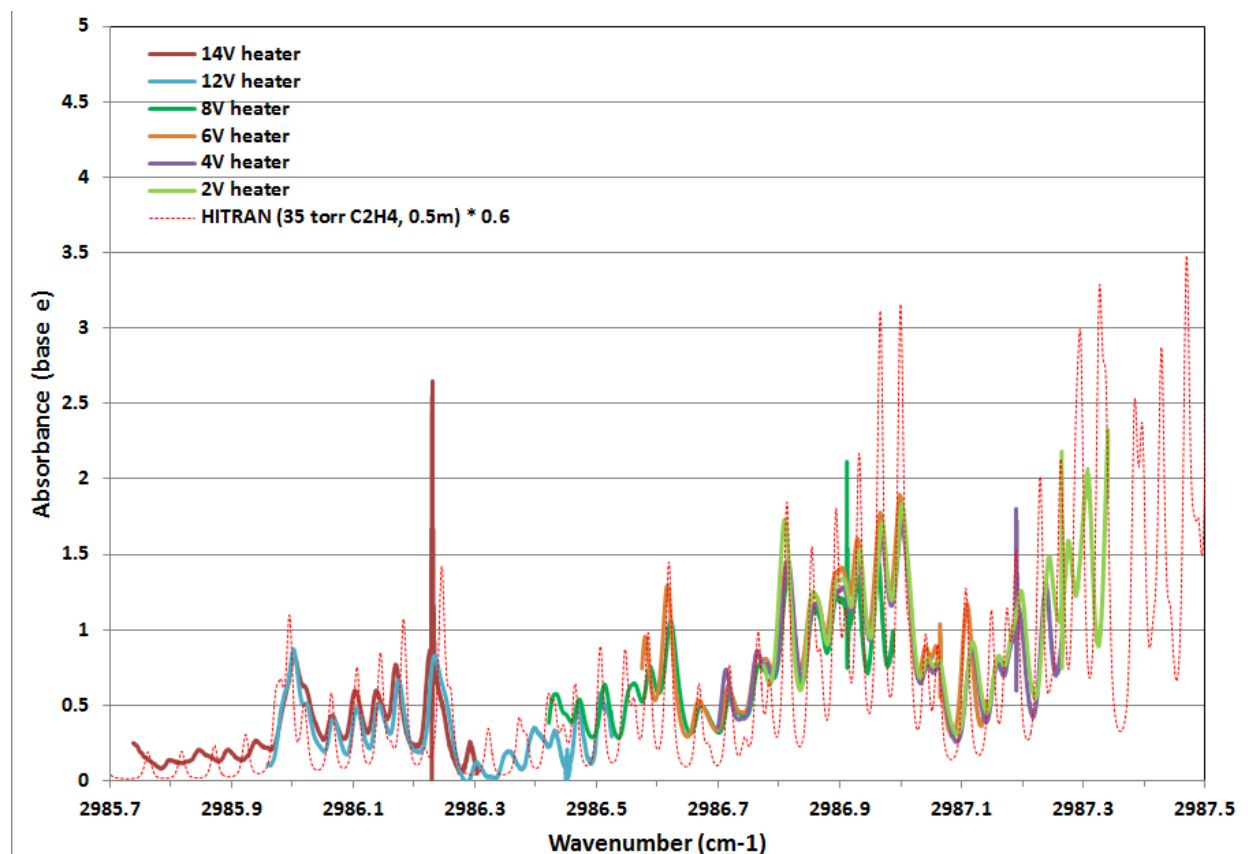


Figure 9. Survey absorption spectra of ethylene at various laser heater setpoints compared to HITRAN simulation.

Recorded as a function of time, each of the peaks in the ethylene spectrum are traversed in approximately 200 ns. Thus, to fully resolve the amplitude of these peaks, our detection system would require a frequency bandwidth of at least 10 MHz. The available detector bandwidth was only 200 kHz, so the peak amplitudes of these features are not accurately recorded. As our intent was only to determine the location of the peak, not its amplitude, this data is sufficient to calibrate the wavelength setpoints for the laser. Similar scans were obtained at fixed temperature setpoints as a function of laser current tuning sine-waves, using a solid Ge etalon, allowing time-dependent data to be transformed accurately into frequency-dependent data. Figure 10 shows an example of such transformed data for group of ethylene transitions around  $2986.9 \text{ cm}^{-1}$ . These data were acquired with 35 Torr of ethylene and a balance of

nitrogen to a total of pressure of 760 Torr, where the individual absorption features as shown in Figure 9 are now blended into single transition approximately  $0.3 \text{ cm}^{-1}$  in width.

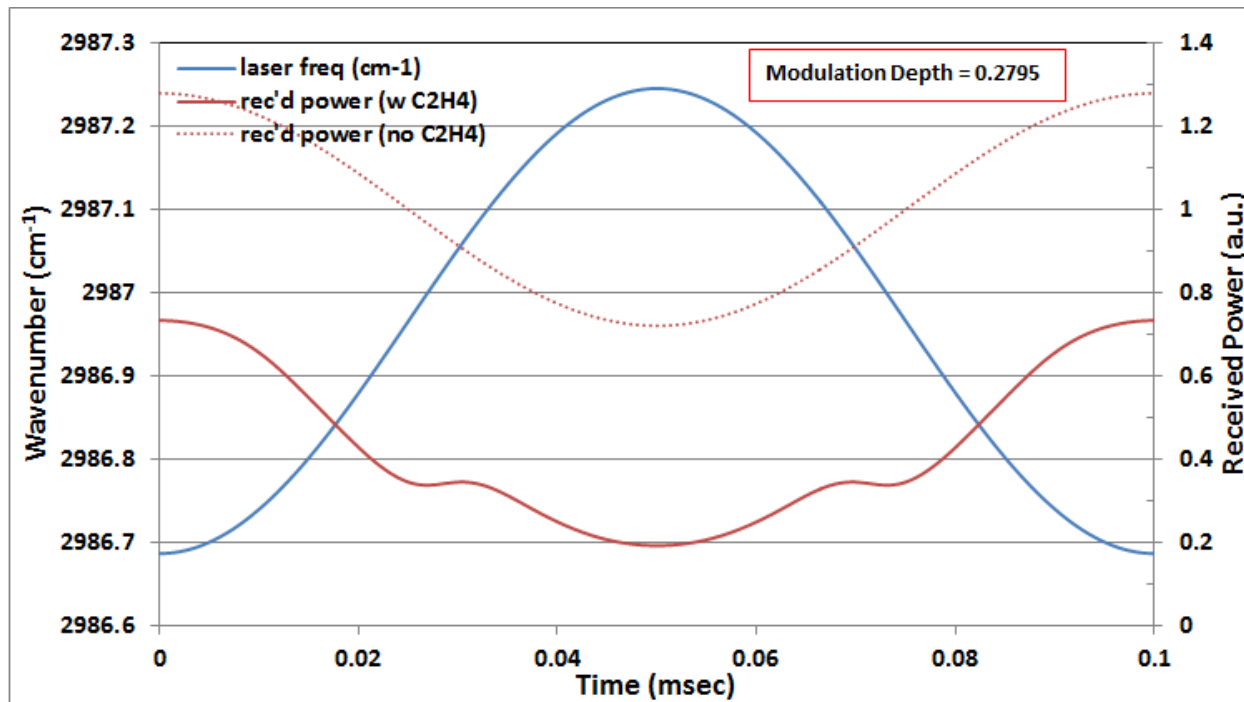


Figure 10. Example laser scan waveform through the absorption with and with-out ethylene at a total cell pressure of 760 Torr (balance nitrogen).

Using the raw absorption data from Figure 10, we can compare the experimental WMS signals as a function of modulation depth with the modeled WMS signals using the HITRAN database. Figure 11 is such a comparison, where we have scaled the experimental 1f and 2f data with a single multiplicative constant to bring the 2f signals into agreement at the lowest modulation depth. The overall agreement as a function of modulation depth is excellent, proving that our simplified model of the WMS process accurately captures the signal behavior – at least for modulation depths up to  $\sim 0.4 \text{ cm}^{-1}$ . The absolute magnitude of the 1f signal is approximately 22% lower than predicted and the reason for this discrepancy is not entirely clear at this time. It does not, however, materially impact the Fuelfinder sensitivity projections: it is simply a scale factor in calibrating the sensor's absolute concentration response.

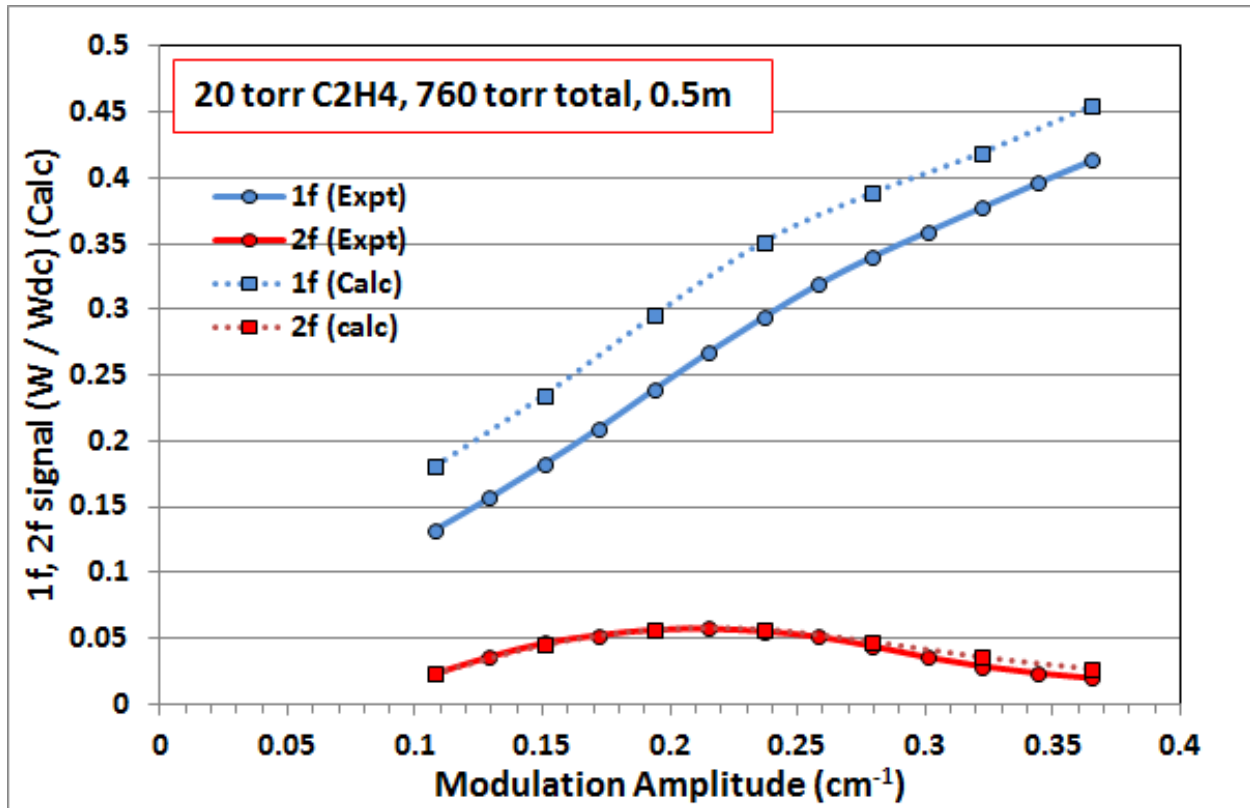


Figure 11. Comparison of experimental (solid) and modeled (dashed) dependence of WMS 1f and 2f signals with laser modulation amplitude using the ethylene absorption feature at  $2986.8 \text{ cm}^{-1}$ .

## 5. ICL Testing

Maxion Technologies (now part of Thorlabs Inc.) was tasked to produce a single-frequency, room-temperature DFB-ICL for use in the program. This task was 100% self-funded by Maxion. Broadband, multi-wavelength ICL's were produced early in the program with output powers in the 10's of mW range in the target spectral regions. However, in the 20 months since November, 2011, Maxion has been unable to produce a single-frequency laser due to processing problems. The program was essentially on-hold for over a year awaiting delivery of the laser.

In March, 2014, however Nanoplus announced the commercial availability of a room-temperature, single-frequency DFB ICL at one of our targeted spectral regions (region b in Fig. 3). We determined that the most efficient conclusion of the program would be to buy one of these lasers and complete a laboratory demonstration of the Fuelfinder sensor. PSI purchased the ICL using our own funds. The laser was powered and temperature-controlled with a SRS LDC500 laser diode controller. The laser output was collimated with a Lightpath Black Diamond asphere lens to  $\sim 5 \text{ mm } 1/e^2$  diameter, and characterized with a Bristol 721 spectrum analyzer and Ophir thermal power meter. As illustrated in Figure 12, injection current tuning ( $-0.165 \text{ cm}^{-1} / \text{mA}$ ) yielded a  $\sim 3 \text{ cm}^{-1}$  range over the singlemode operating regime, well beyond

the optimum tuning range indicated by our simulation. Temperature tuning yielded an  $\sim 1 \text{ cm}^{-1}$  shift for every  $3^\circ\text{C}$  ( $0.268 \text{ cm}^{-1} / ^\circ\text{C}$ ). Nominal output power at 40mA dc operating current was  $\sim 5 \text{ mW}$ .

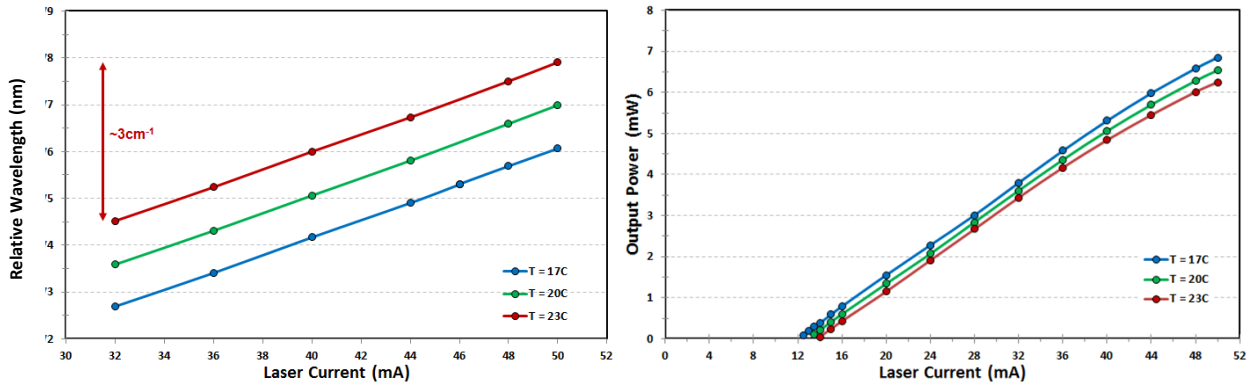


Figure 12. (left) Laser spectral sensitivity to operating temperature and drive current. (right) Laser output power versus operating temperature and drive current.

## 6. Laboratory Demonstration of Fuelfinder Response

The laser was inserted into a laboratory prototype transceiver comprised of the laser, a fast ( $f/2$ ) 4.5" diameter aluminum mirror, and a 1mm InAs detector with a built-in preamplifier operating at room temperature. The laser beam was delivered across the room ( $\sim 18 \text{ ft}$ ) and scattered off a rough aluminum plate. This experimental setup is illustrated schematically in Figure 13. With a detector responsivity of  $1.4 \text{ A/W}$  and a recorded average signal of  $\sim 45 \text{ mV}$ , the collected backscattered laser power was  $\sim 30 \mu\text{W}$ . The laser was run in most cases at a dc laser current of 40 mA and a 1 kHz, 20 mA<sub>pk-pk</sub> modulation.

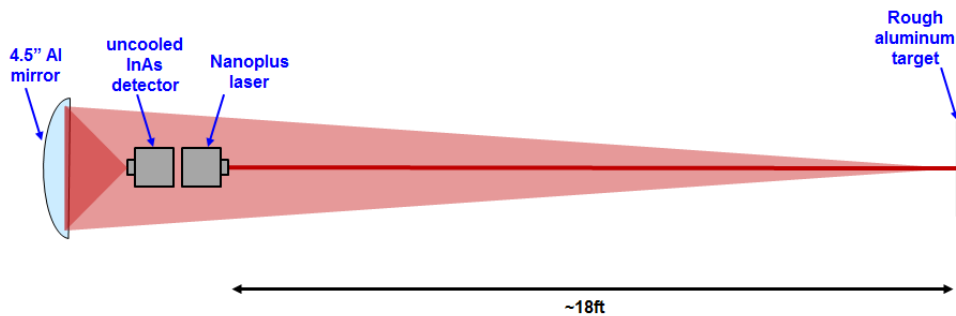


Figure 13. Schematic of laboratory prototype Fuelfinder backscatter experiment.

Figure 14 illustrates typical oscilloscope recordings over one period of the detected signal. The plot is for 100 trace averaging, equivalent to 0.1s averaging or 10 Hz data rate. The blue trace shows the transmission through a  $0.048\text{ cm}^{-1}$  period Ge etalon. At this tuning rate, the 45 fringes indicate a total tuning range of  $2.16\text{ cm}^{-1}$  over this current ramp (or a modulation depth of  $1.08\text{ cm}^{-1}$ ). The phase shift between the frequency and amplitude modulation is typical of current tuned lasers.

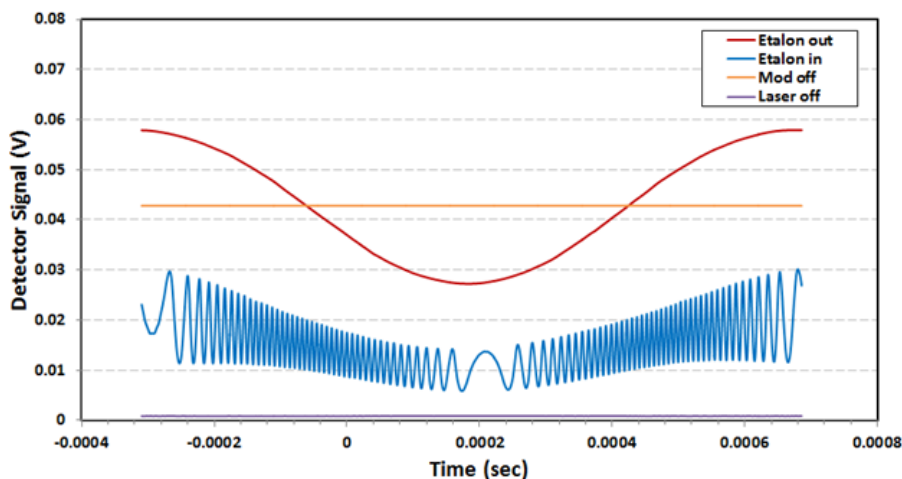


Figure 14. Recorded traces of the ICL scatter signals with (blue) and without (red) an etalon in the beam path.

Fixed path-integrated concentrations of gasoline were then interrogated by placing a 20 cm long cell in front of the outgoing laser beam. The cell was fitted with 1" diameter  $\text{CaF}_2$  end windows and connectorized to flow gas mixtures. A lock-in amplifier was used to record both the  $1f$  (1k Hz) signal and phase (relative to the modulation reference waveform) and the  $2f$  signal and phase. Two mass-flow metered  $\text{N}_2$  flows were employed and mixed prior to entering the cell. The first was a very low flow (0-15 sccm) that was carrying gasoline vapor (by bubbling it through a graduated cylinder with 150 ml of gasoline in it). The second flow (500-1500 sccm) was employed to dilute the gasoline-carrying flow. Comparison of measured absorbance signals to reference data suggests that the bubbler was achieving a consistent  $\sim 60\%$  saturation of the carrying gas with gasoline vapor. Quantitative variation of gasoline concentration was achieved by varying the ratio of the two gas flows. Figure 15 is a photo of the laboratory prototype and also illustrates the components of this flow system for gasoline vapor measurements.

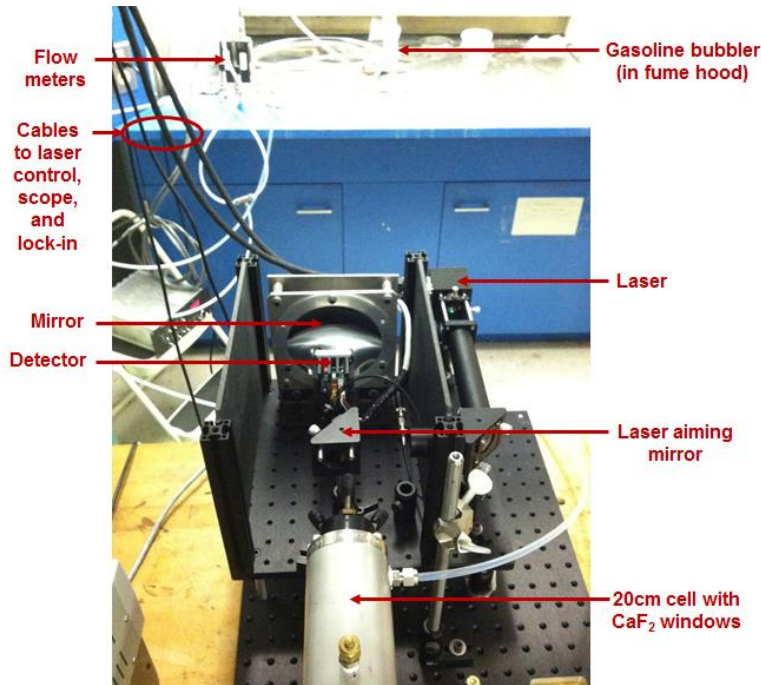


Figure 15. Photo of the laboratory prototype transceiver (cover partially off) with 2 cm optical cell in front of the outgoing beam, and connected to the gasoline vapor delivery system (background).

Measurements were performed with the laser tuned to both spectral region b and the nearby negative inflection in the gasoline spectrum. Also, to minimize the water feature contribution, the backscatter path was shortened to ~4.5 ft.

Figure 16 plots scope traces (top) at a few different gasoline vapor concentrations and the resultant calculated absorbance (bottom). This plot runs over one period, from lower frequency (higher laser intensity) to higher frequency (lower laser intensity) back to lower frequency. The expected broad slope of the absorbance curve is observed (~10% change over the modulation range).

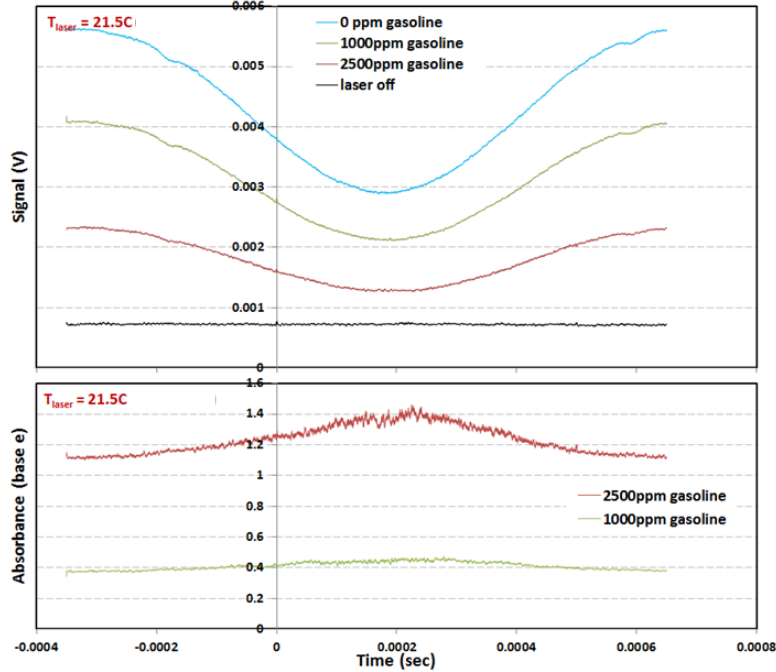


Figure 16. (top) Recorded oscilloscope traces (100-sweep (0.1sec) average) for 4 noted conditions. (bottom) Calculated absorbance for the two conditions with gasoline in the path of the laser beam.

In Figure 17, the data of Figure 16 are fitted to pure sine waves, and the residual differences between the data and the fits are plotted. The residuals illustrate features that contribute to a  $2f$  signal, even with no gasoline vapor. These features result from: a) excessive laser modulation that inadvertently encompassed the water vapor absorption line at  $2461.7 \text{ cm}^{-1}$ , and b) non-linear laser amplitude response at the higher currents (see Fig. 12 right), known as Residual Amplitude Modulation (RAM). The consequence of these features is an offset in the measurement of gasoline vapor concentration.

To quantify the sensitivity to gasoline vapor and the offsets, we provided the sensor signals along with a reference waveform from the modulation input to the laser controller, as inputs to an analog lock-in amplifier. The lock-in generated outputs of  $1f$  and the  $2f$  quadrature components ( $2f(i) = |2f| \cos(\theta_{2f})$ ,  $2f(q) = |2f| \sin(\theta_{2f})$ ). Figure 18 plots  $[2f(q)/1f]/[2f(i)/1f]$ , illustrating the magnitude and phase of the  $2f$  signals at different conditions. The magnitude increases with increasing gasoline vapor concentration, while the phase remains constant, verifying that the sensor is responding correctly to spectral absorption.

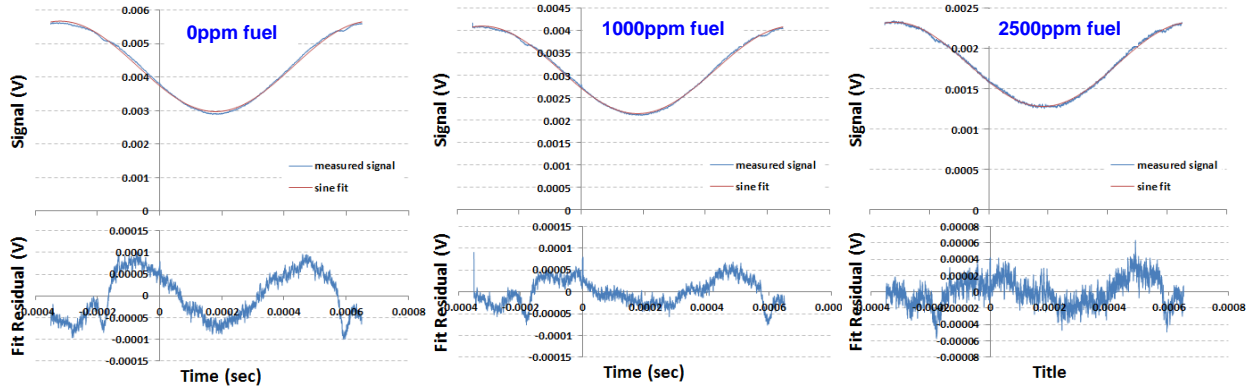


Figure 17. (top) Recorded oscilloscope traces (blue) (100-sweep (0.1 sec) average) and sine fit (red) for 3 different fuel concentrations in the optical cell. (bottom) Residuals from the fits. Note the  $2f$  content. Also evident is the sharp water feature at the wings.

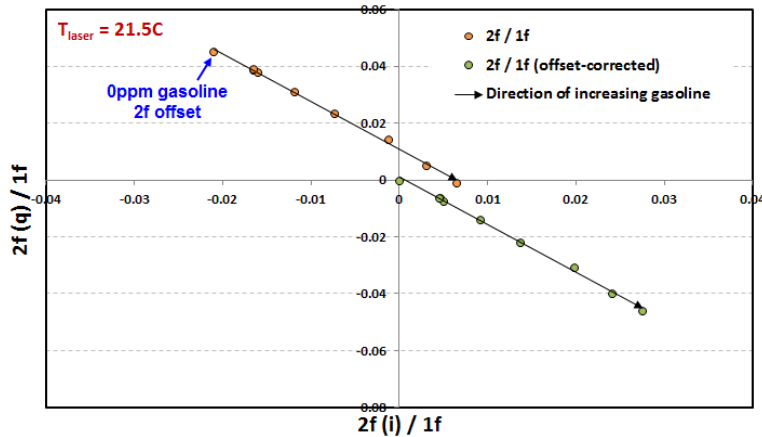


Figure 18. Lock-in quadrature signals for  $2f$  at different gasoline concentrations. The signals are normalized by the simultaneously recorded  $1f$  magnitude. Signals at the zero gasoline condition ( $2f/1f$  “offset”) are indicated and increasing gasoline directs the signal in the direction of the arrows. The green data points are simply the orange data with the offset subtracted.

Figure 19 plots the offset-corrected  $2f/1f$  signal magnitudes from Figure 18 against the calculated concentrations for gasoline vapor in the optical cell. The large uncertainty in the calculated gasoline vapor concentration is due to the low flow rates (and resultant high uncertainty in the mass flow values) used. Flow accuracy is estimated at  $\pm 0.5$  sccm and some drift was evident, yielding a total estimated flow uncertainty of  $\pm 0.75$  sccm.

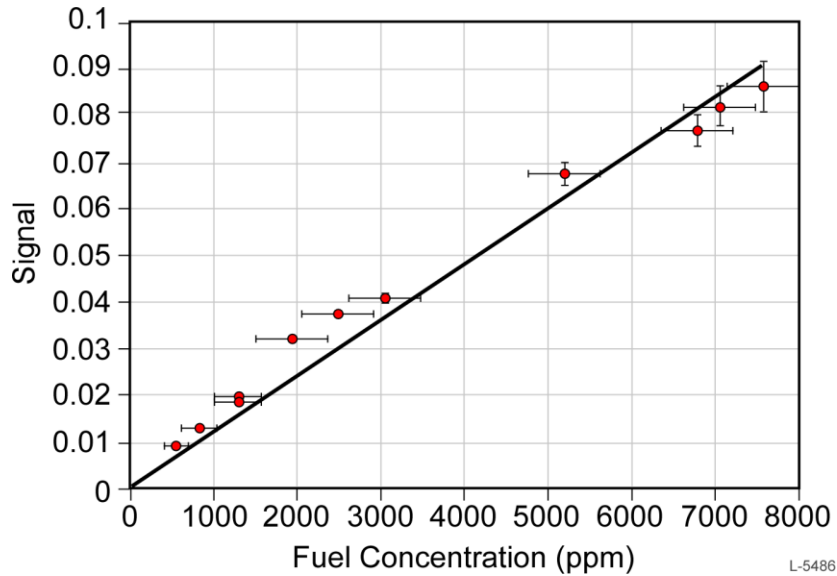


Figure 19. Plot of offset-corrected  $2f / 1f$  signals versus calculated gasoline concentration in the optical cell

Using the uncertainty in the measured signal ratio at the low fuel concentration data points and the slope of the response curve of the data, we estimate a gasoline vapor detection limit of 8 ppm-m. This is comparable to the predicted sensitivity of Figure 5, providing further confirmation of the validity of our simulation tool. In practical application, variation in path-integrated water content (as the sensor is aimed about) will limit the reliable sensitivity. Figure 4 indicates the signal from 600,000 ppm  $H_2O$  is approximately as strong as 17 ppm-m gasoline. This would indicate 50ppm-m gasoline is measurable with a  $S/N \sim 3$ .

## 7. Summary and Suggested Next Steps

This program demonstrated the first room-temperature TDLAS sensor for the detection of gasoline vapor. In a stand-off geometry at a distance of 1.4 m, detection limits of 8 ppm-m were demonstrated for a fixed pathlength, in stable laboratory conditions, consistent with detailed instrument simulations and our expectations from the time of the proposal.

Unanticipated lengthy delays in obtaining a suitable room-temperature, single-frequency ICL eliminated the possibility of completing measurements of gasoline vapor above buried fuel pools or simulated leak scenarios. The emergence of a commercial source of the ICL and the encouraging laboratory results suggest that a follow-on effort devoted to characterizing the gasoline vapor plumes from underground leaks is warranted. The goal of this follow-on would be to understand the fate of volatile gasoline components through a variety of soil conditions and leak scenarios. It would also prove the feasibility of detecting these vapor plumes before visible liquid or other surface signatures are evident.

**References:**

1. Physical Properties of Gasoline Components (EPA):  
<http://www.epa.gov/athens/learn2model/part-two/onsite/sparcproperties.html>
2. CDC Toxicological Profile – Gasoline (Ch. 5.3 – Potential for Human Exposure (Environmental Fate)): <http://www.atsdr.cdc.gov/ToxProfiles/tp.asp?id=468&tid=83>